Published in final edited form as:
Biomaterials. 2010 July ; 31(19): 5083–5090. doi:10.1016/j.biomaterials.2010.03.020.

Biocompatibility of Polymer Grafted Core/Shell Iron/Carbon Nanoparticles

Qingxin Mu[1,2], **Lei Yang**[2], **James C. Davis**[2], **Raviraj Vankayala**[3], **Kuo Chu Hwang**[3], **Jincai Zhao**[4], and **Bing Yan**[1,2,*]

[1]School of Chemistry and Chemical Engineering, Shandong University, Jinan, 250100, China

[2]St. Jude Children's Research Hospital, Memphis, Tennessee, 38105 U.S.A.

[3]Department of Chemistry, National Tsing Hua University, Hsinchu, Taiwan

[4]Institute of Chemistry, Chinese Academy of Sciences, Beijing 100080, China

Abstract

For biomedical applications, emerging nanostructures requires stringent evaluations for their biocompatibility. Core/shell iron/carbon nanoparticles (Fe@CNPs) are nanomaterials that have potential applications in magnetic resonance imaging (MRI), magnetic hyperthermia and drug delivery. However, their interactions with biological systems are totally unknown. To evaluate their potential cellular perturbations and explore the relationships between their biocompatibility and surface chemistry, we synthesized polymer grafted Fe@CNPs with diverse chemistry modifications on surface and investigated their dynamic cellular responses, cell uptake, oxidative stress and their effects on cell apoptosis and cell cycle. The results show that biocompatibility of Fe@CNPs is both surface chemistry dependent and cell type specific. Except for the carboxyl modified Fe@CNPs, all other Fe@CNPs present low toxicity and can be used for further functionalization and in a wide range of biomedical applications.

Keywords

nanomaterials; core/shell nanoparticles; biocompatibility; RT-CES; cytotoxicity

1. Introduction

Investigation of interactions between emerging nanoconstructs and biological systems is of utmost importance in order to develop safe nanotechnology for biomedical applications [1]. Core/shell iron/carbon nanoparticles (Fe@CNPs) are functional nanomaterials with promising applications in biomedical sciences [2,3]. They consist of metal iron as core and graphene coating layers with reactive linkers for chemistry modifications. Besides the magnetic properties and near-IR adsorption and emission properties of graphene coating on Fe@CNPs, the graphene layers also protect iron core from air oxidation, water hydration and acid corrosion. Furthermore, the graphene can also be functionalized with small molecules [4] or

*To whom correspondence should be addressed, bing.yan@stjude.org.

biomacromolecules [5] for cell targeting and other functions. Therefore, they can be used as promising biomedical nanodevices, such as magnetic resonance imaging (MRI) contrast agents, tumor targeting hyperthermia agents and drug delivery carriers. Fe@CNPs can now be produced in high purity and large quantity [2,3]. However, the interactions of Fe@CNPs with biological systems are totally unknown. As a functional nanomaterial for biomedical applications, its biological impacts need to be addressed.

Although cellular effects of Fe@CNPs are unknown, biological perturbations of other carbon-based nanomaterials have been reported [6–14]. Based on previous reports and our own observations, these materials may have toxicity. For instance, pristine carbon nanotubes (CNTs) can induce cell apoptosis by activating MAPK and NF-κB signaling pathways [9]. We discovered that water soluble carboxylated single walled carbon nanotube (SWCNT-COOH) inhibited cell proliferation by suppressing BMP signaling [10]. Fullerenes may cause lipid peroxidation under normal cell culture condition with room light [13]. The biological activities of nanomaterials are mostly dictated by their surface properties [15–17]. Therefore, the toxicity can possibly be remedied through surface chemistry modifications. Using a nano-combinatorial chemistry approach, we proved this hypothesis by reducing CNTs' protein binding, cytotoxicity and immune perturbations [18]. To identify the suitability of Fe@CNPs carrying different surface chemistry in various biomedical applications, we studied their interactions with mammalian cells by monitoring their cell uptake, effects on cellular oxidative stress, cell proliferation, apoptosis and cell cycle.

2. Materials and methods

2.1. Cell cultures, materials and reagents

HEK293 (human embryonic kidney epithelial) and C33A (human cervical carcinoma epithelial) cells (from ATCC) were grown in Dulbecco's Minimum Essential Medium (DMEM, Gibco, Grand Island, NY, USA) supplemented with 10% heat-inactivated fetal bovine serum (Invitrogen, Carlsbad, CA, USA), 2 mM L-glutamine, 100 μg/mL penicillin and 100 U/mL streptomycin. The cells were grown in a humidified incubator at 37 °C (95% humidity, 5% CO_2). Guava Nexin-V apoptosis and Guava cell cycle reagents were purchased from Millipore Corp. (Billerica, MA, USA). Other chemicals were purchased from Sigma Aldrich (St. Louis, MO, USA).

2.2. Synthesis of polymer coated Fe@CNPs

2.2.1. CNPA—In a typical experiment, Fe@CNPs (50 mg) was suspended in an aqueous solution (8 ml) containing acrylic acid (AA, 1 mL) monomer. The solution was then ultrasonicated in a bath-type ultrasonicator for 2 min to help disperse the core/shell iron/carbon nanoparticles. A tetrahydrofuran (THF) solution (0.25 mL) containing benzoyl peroxide (22.5 mg) was added to the solution, followed by ultrasonication for an additional 10 min. This process was repeated 4 or 5 times with a total amount of 90–120 mg benzoyl peroxide added. The final solution was then diluted with deionized water, filtered through a Nylon 66 (0.45 μm) membrane, and washed with deionized water several times to thoroughly remove free, unbound PAA polymers from CNPAs.

2.2.2. CNPB—In a typical experiment, Fe@CNPs (50 mg) was suspended in toluene (10 ml) containing N-vinyl pyrrolidone (2 mL) monomer. The solution was then ultrasonicated in a bath-type ultrasonicator for 2 min to help disperse the core/shell iron/carbon nanoparticles. A tetrahydrofuran (THF) solution (0.25 mL) containing benzoyl peroxide (22.5 mg) was added to the solution, followed by ultrasonication for an additional 10 min. This process was repeated 8 or 9 times with a total amount of 150–180 mg benzoyl peroxide added. The final solution was then diluted with ethanol, filtered through Nylon 66 (0.45 μm) membrane, and washed

with deionized water several times to thoroughly remove free, unbound PVP polymers from CNPBs.

2.2.3. CNPC—In a typical experiment, Fe@CNPs (50mg) was suspended in ethanol 20 ml) containing 0.1 M 2-aminoethyl methacrylate monomer. The solution was then ultrasonicated in a bath-type ultrasonicator for 2 min to help disperse the core/shell iron/carbon nanoparticles. A tetrahydrofuran (THF) solution (0.25 mL) containing benzoyl peroxide (22.5 mg) was added to the solution, followed by ultrasonication for an additional 10 min. This process was repeated 4 or 5 times with a total amount of 90–120 mg benzoyl peroxide added. The final solution was then diluted with ethanol, filtered through Nylon 66 (0.45 μm) membrane, and washed with deionized water several times to thoroughly remove free, unbound PAEMA polymers from CNPCs.

2.2.4. CNPD—In a typical experiment, Fe@CNPs (50 mg) was suspended in an aqueous solution (8 ml) containing 2-hydroxethyl methacrylate (2 mL) monomer. The solution was then ultrasonicated in a bath-type ultrasonicator for 2 min to help disperse the core/shell iron/carbon nanoparticles. A tetrahydrofuran (THF) solution (0.25 mL) containing benzoyl peroxide (22.5 mg) was added to the solution, followed by ultrasonication for an additional 10 min. This process was repeated 4 or 5 times with a total amount of 90–120 mg benzoyl peroxide added. The final solution was then diluted with deionized water, filtered through a Nylon 66 (0.45 μm) membrane, and washed with deionized water several times to thoroughly remove free, unbound PHEA polymers from CNPDs.

2.3. Characterizations of Fe@CNPs

The structures of Fe@CNPs were characterized using a transmission electron microscope (TEM) (Jeol JEM-2100F, 200 kV) operated at 200 kV voltage. The crystalline structure of the Fe nanoparticles core in the Fe@CNPs were determined by x-ray diffraction (XRD) measurements in the range of 20° and 80° using Cu Kα (λ= 0.15406 nm) radiation as the light source and data processed using a M18XCE program from MAC Science Co., Ltd. Fourier transformed infrared (FT-IR) spectra of surface-functionalized Fe@CNPs were measured using a FT-IR spectrometer (Bomem, model DA8.3) in the range of 500–4000 cm^{-1}. The zeta potential of nanoparticles was determined using Zetasizer Nano-Z (Malvern Instruments, Worcestershire, UK). The analysis was performed at 25.0 ± 0.2°C using sample solutions in de-ionized distilled water. The zeta potential was an average of three independent measurements.

2.4. Real-time cell-based electronic sensing (RT-CES) assay

Multi E-Plate (MP) System (ACEA Biosciences, San Diego, CA) was used for the assay. The Cell Index (CI) is derived from the cell status-based cell-electrode impedance. The CI is calculated by equation (1):

$$CI = \max_{i=1,\ldots,N}\left(\frac{Rcell(fi)}{Rb(fi)} - 1\right) \quad (1)$$

Where Rb(f) and Rcell(f) are the frequency-dependent electrode resistances of background and cells, N is the number of the frequency points at which the impedance is measured. The CI reflects a gross condition of cell growth, such as cell number, cell adhesion, cell spreading, and cell morphological changes. The assay was performed as previously described [10, 19]. Briefly, volumes of 50 μL of media was added to wells in 96-well E-plates to obtain background readings followed by the addition of 100 μL of cell suspension (HEK293 10,000 cells/well and C33A 40,000 cells/well). The cells were allowed to attach and spread on the sensors until the

cell index reaches ~1.0 before adding Fe@CNPs. Fe@CNPs were suspended in cell culture medium as stock solutions (800 μg/mL). They were added into cells with the final concentration of 25 and 50 μg/mL. The data points were collected automatically every 20 min. Each concentration was triplicated.

2.5. Transmission electron microscopy (TEM) observation of cell uptake

The method was adapted from previously described [10,11,19]. C33A cells were treated with 400 μg/mL CNPP or CNPA for 24 hours. Then cells were washed three times with PBS and fixed in 2.5% glutaraldehyde in 0.1M sodium cacodylate buffer (pH 7.4) for 1 hour at room temperature, then rinsed in three changes of same buffer. Cells were then post fixed one hour in 2% osmium tetraoxide with 3% potassium ferricyanide, rinsed in three changes of same buffer, next enbloc staining with a 2% aqueous uranyl acetate solution and dehydration through a graded series of alcohol (50%, 70%, 80%, 95%, 100%). They were then put into two changes of propylene oxide, a series of propylene/epon dilutions and embedded. The thin (70 nm) sections were cut on a Leica UC6 ultramicrotome and images were taken on a JEOL 1200 EX (JEOL, Ltd. Tokyo, Japan) using an AMT 2k digital Camera.

2.6. Flow cytometry analyses

Flow cytometry analyses were performed on a Guava® EasyCyte™ Mini flow cytometry system (Millipore, Billerica, MA).

2.6.1. Reactive oxygen species (ROS) generation—HEK293 and C33A cells were seeded into 12-well plates with the density of 200,000 cells per well. Twenty four hours later, Fe@CNPs stock solutions were added into cells with the final concentration of 50 and 400 μg/mL, respectively. Cells were incubated with nanoparticles for 24 hours. Cell culture medium was then replaced with Dihydroethidium (DHE) solution (5 μM in cell culture medium) and incubated with cells for 30 min at 37 °C. Cells were then trypsinized and aspirated, followed by flow cytometry analysis. Red fluorescence was monitored.

2.6.2 Annexin-V apoptosis assay—HEK293 and C33A cells were seeded into 12-well plates with the density of 200,000 cells per well. Twenty four hours later, Fe@CNPs stock solutions were added into cells with the final concentration of 50 and 400 μg/mL, respectively. Cells were incubated with nanoparticles for 24 hours. Cells were then trypsinized, aspirated and suspended in 2 mL PBS. Cells were further incubated with Guava Nexin-V reagent for 20 min at room temperature in darkness (100 μL cell suspension was mixed with 100 μL reagent), followed by flow cytometry analysis.

2.6.3 Cell cycle analysis—HEK293 and C33A cells were seeded into 6-well plates with the density of 500,000 cells per well. Twenty four hours later, Fe@CNPs stock solutions were added into cells with the final concentration of 50 and 400 μg/mL, respectively. Cells were incubated with nanoparticles for 24 hours. Cells were then trypsinized, aspirated and counted, followed by being fixed in 5 mL ethanol for 4 hours at 4 °C. Cells were centrifuged and washed once with PBS; and equal numbers of cells were then re-suspended in 200 μL Guava cell cycle reagent. Cells were incubated with reagent for 30 min at room temperature in darkness prior to flow cytometry analysis.

3. Results and discussion

3.1. Characterization of Fe@CNPs

The pristine Fe@CNPs was modified with different surface functionalities in this work (Figure 1A). These hydrophilic functionalities were chosen to make Fe@CNPs possess negative (acid), positive (amine), zwitterionic (vinyl pyrolidone) (Huang wrote this), and neutral (alcohol)

charges at the physiological pH, which was used in cellular experiments. The TEM images in Figure 1B show that the pristine Fe@CNPs have well-graphitized graphene shells with an iron nanoparticle core in the center. The graphene shells can protect the iron nanoparticles from air oxidation in diverse biomedical applications and from acid etching in surface modification processes. After surface functionalization, Fe@CNPs was separated from free polymers in the solution by centrifugation and several wash-centrifuge cycles. After surface modification, Fe@CNPs became soluble in water. The surface functional groups were characterized by FT-IR (see Figure 1D). For CNPA, the characteristic bands of the acrylic acid moieties appear at 3300~3600 cm^{-1} (strong and broad band for the acid -OH stretching), and 1730 cm^{-1} (strong, for the acid >C=O stretching). For CNPB, the characteristic bands of the pyrolidone moieties appear at 3427 cm^{-1} (for broad hydroxyl O-H stretching), 2927 cm^{-1} (weak band for alkyl C-H stretching), and 1644 cm^{-1} (strong band for the lactam >C=O stretching). The presence of the hydroxyl signal is due to the ketone-enol form tautomerization of the pyrolidone moiety. For CNPC, the characteristic bands of the primary amine moieties appear at 2960~3200 cm^{-1} (for symmetric and asymmetric N-H stretching), and 1748 cm^{-1} (for ester >C=O stretching). For CNPD, the characteristic strong and broad bands for the alkyl alcohol moiety appears at 3200~3600 cm^{-1}, in accompany with strong stretching signal at 1740 cm^{-1} for the ester >C=O. To characterize the structure of the encapsulated iron nanoparticle, powder x-ray diffraction measurements were also performed and results shown in Figure 1E. All five samples (CNPP, CNPA, CNPB, CNPC, and CNPD) show similar diffraction patterns. By comparison with the data in JCPDS, the diffraction peaks at 25.7, 43.5, 44.4, 50.6 and 64.8 were assigned to diffraction signals from the graphene (002), γ-Fe(111), α-Fe(110), γ-Fe(200), and α-Fe(200) crystalline facets, respectively (see also the assignments in the Figure 1E). The XRD measurements showed that the encapsulated iron nanoparticles could exist in either alpha- (with body-centered cubic crystalline structure) or gamma- (with face-centered cubic crystalline structure) form, or both. Surface functionalization occurs on the outmost graphene layer, and does change or affect the crystalline structures of the inner graphene layers and of the encapsulated iron nanoparticle. The surface charges of Fe@CNPs in aqueous solution were reflected in their ζ potentials (Figure 1C). Depending on their surface modifications, they exhibit various surface charges ranging from positive (CNPC) through neutral (CNPP) to negative (CNPA, CNPB and CNPD).

3.2. Dynamic cellular responses of Fe@CNPs

The interactions of nanoparticles with human cells are dynamic processes. However, traditional cytotoxicity assays are limited to end point assays. Important intermediate processes may be missed in these assays. Furthermore, most cytotoxicity assays are based on measuring optical signals and strong UV-Vis absorbing nanoparticles exhibit strong interference in these assays [20–22]. To avoid these problems, we applied a real-time cell electronic sensing assay (RT-CES) [19,23,24] to monitor the dynamic cellular responses to Fe@CNPs. In this work, we evaluated Fe@CNP's cellular effects on two human cell lines, human embryonic kidney cells (HEK293) and human cervical carcinoma cells (C33A). Figure 2 shows the time-dependent cell responses to different nanoparticles (Figure 2). The normalized cell index reflects the gross cell growth status [24]. For HEK293 cells, the growth at early stage of nanoparticles exposure was affected more than later phase. Except for CNPA, cells had a moderate recovery and adaptation even under the stress of all other Fe@CNPs. In contrast, all Fe@CNPs more or less suppressed the growth of C33A at the later stage. Only CNPA displayed strongest cell growth perturbation to both cell lines. The results show that despite some cell type-specific responses the surface chemistry plays a major role in perturbing cell proliferation. In previous reports and our own studies, carboxylated nanoparticles often showed stronger biological activities. Carboxylated multi-walled carbon nanotubes (MWCNT-COOH) have the strongest binding affinity to proteins over other types of surface chemistry [16]; SWCNT-COOH inhibits cell growth through a BMP signaling suppression mechanism [10]; magnetic nanoparticles (MNPs)

with carboxyl modification can inhibit cell growth [19]. Further chemistry modifications on carboxyl group reduced toxicity of nanoparticles [16].

3.3. Cell uptake

To account for Fe@CNPs' effects on cell proliferation, it is desirable to examine whether nanoparticles can be taken up by human cell. The cell uptake was monitored by TEM after cells were incubated with Fe@CNPs for 1 h at 37°C. Results show that both pristine and modified nanoparticles can enter cells. Both nanoparticles were found in cytoplasmic vesicles (Fig. 3). Figure 3B shows that a cluster of CNPA was attacking cytoplasmic membrane (upper arrow) and was about to enter the cell. TEM results are consistent with the likelihood that Fe@CNPs entered cells mainly through endocytosis. On the basis of current knowledge, all types of spherical nanoparticles, no matter carbon nanostructures or magnetic nanoparticles enter cells through endocytosis [10,11,19,25]. Nanoparticles are then recruited into lysosome and exocytosed. It is clearly seen from TEM that Fe@CNP can enter cells freely indicating that they can be used for future drug delivery or cell labeling.

3.4. ROS generation

Exposure to nanoparticles may cause generation of reactive oxygen species (ROS) in cells. The oxidative stress is a widely accepted mechanism for nanoparticle toxicity [9,13]. To examine the induction of oxidative stress by Fe@CNPs with diverse surface chemistry, we examined cellular ROS generation by flow cytometry using a reductive reagent, dihydroethidium. This reagent reacts with ROS in cells and is subsequently oxidized to fluorescent ethidium. Cells were treated with nanoparticles for 24 h with a low (50 μg/mL) and a high dose (400 μg/mL), respectively. Results (Figure 4) show that, all Fe@CNPs caused a certain degree of oxidative stress as compared to control (red filled histograms) at the high dose in both cell lines. When treated at the low dose, only HEK293 cells generated ROS while C33A cells were not affected. These results indicate that HEK293 cells are more sensitive to Fe@CNPs than C33A cells. Interestingly, pristine Fe@CNPs don't generate ROS in HEK293 cells (Figure 4A) at the low dose, however, Fe@CNPs with surface modifications can induce slight oxidative stress in the same cell line. This is probably because that surface modification makes Fe@CNPs better dispersed and increases the chance of their interactions with cells. Similar phenomenon was also observed in surface-modified silver nanoparticles [26]. Furthermore, surface characteristics of particles may modify ROS generation in human cells such as quartz particles [27]. In contrast, no significant difference in ROS intensity (peak shift in Fig. 4) generated by surface modified Fe@CNPs (CNPA~D) was observed at various doses. Therefore, material components eventually play an important role in such effect.

3.5. Annexin-V apoptosis assay

Cell behavior is controlled by molecular events inside cell and ROS has been identified as an inducer of cell apoptosis [9,28,29]. Therefore, we determined Fe@CNP-induced cell apoptosis using Annexin-V by flow cytometry. Cells were treated with nanoparticles under the same conditions as oxidative stress experiments. Results show that only high dose CNPA generated 11.3% of apoptotic HEK293 cells. This result confirms that only CNPA shows cytotoxicity. Results indicate that most functionalized Fe@CNPs do not induce cell apoptosis although they induced ROS to the similar degree. Therefore, oxidative stress is not the inducer factor for cell apoptosis induced by Fe@CNPs. Furthermore, various perturbations of Fe@CNPs on cell proliferation (Figure 2) seem not correlated with cell apoptosis induced by nanoparticles with the exception of CNPA. Considering RT-CES measures a gross cell status including cell number, shape and spreading [24], other Fe@CNPs may only induce morphological changes or perturb cell growth without killing cells.

3.6. Cell cycle analysis

Nanoparticle may perturb celluar signaling events and may affect cell cycle and eventually the cell proliferation [30,31]. To comprehensively evaluate the biological activities of Fe@CNPs, we examined their effects Fe@CNPs on cell cycle in both HEK293 and C33A cells. Cell cycle was analyzed under the same condition as oxidative stress and Annexin-V assays. Results show that, at low dose, Fe@CNPs had no effect on cell cycle distribution in both cell lines. At the high dose, all Fe@CNPs induced G0/G1 arrest and G2/M decrease in HEK293 cells. Among them, CNPA showed the most effects on cell cycle. Therefore, effects of Fe@CNPs on HEK293 proliferation (Figure 2) can be explained by their interference on cell cycle. All nanoparticles showed much less affect on C33A cells at both low and high doses. This indicates that the effect of Fe@CNPs on cell cycle is cell-type specific. In the same cell line, surface chemistry plays the major role in determining such effect.

4. Conclusions

To apply Fe@CNP materials in a wide range of biomedical practices, we investigated their biocompatibility by designing and synthesizing Fe@CNPs with diverse surface chemistry and comprehensively examining their cellular perturbation including dynamic cellular responses, cell uptake, oxidative stress, induction of cell apoptosis and influence on cell cycle. All data support that the cellular responses of Fe@CNPs are both surface-chemistry dependent and cell type specific. Only the carboxlyated Fe@CNPs exhibited consistent toxicity at a high dose. Other Fe@CNPs examined here are non-cytotoxic. Fe@CNPs have advantages over plain carbon or metal nanoparticles. Surface chemistry modifications on these nanoparticles make them more soluble in aqueous solution and suitable candidates for nanomedicine applications. On the basis of our examinations, the selected functional nanomaterials from this work can be further utilized in various biomedical fields.

Acknowledgments

We thank Ms. Linda Mann (Cell and tissue imaging, St. Jude Children's Research Hospital) for the technical assistance on TEM in cell uptake study. This work was supported by the National Basic Research Program of China (973 Program 2010CB933504), National Cancer Institute (P30CA027165), the American Lebanese Syrian Associated Charities (ALSAC), and St. Jude Children's Research Hospital.

References

1. Maynard AD, Aitken RJ, Butz T, Colvin V, Donaldson K, Oberdorster G, et al. Safe handling of nanotechnology. Nature 2006;444(7117):267–269. [PubMed: 17108940]
2. Hsin YL, Lin CF, Liang YC, Hwang KC, Horng JC, Ho JAA, et al. Microwave arcing induced formation and growth mechanisms of core/shell metal/carbon nanoparticles in organic solutions. Adv Funct Mater 2008;18(14):2048–2056.
3. Liang YC, Hwang KC, Lo SC. Solid-state microwave-arcing-induced formation and surface functionalization of core/shell metal/carbon nanoparticles. Small 2008;4(4):405–409. [PubMed: 18383573]
4. Liu Z, Robinson JT, Sun XM, Dai HJ. PEGylated nanographene oxide for delivery of water-insoluble cancer drugs. J Am Chem Soc 2008;130(33):10876–10877. [PubMed: 18661992]
5. Gao LZ, Nie L, Wang TH, Qin YJ, Guo ZX, Yang DL, et al. Carbon nanotube delivery of the GFP gene into mammalian cells. ChemBioChem 2006;7(2):239–242. [PubMed: 16370018]
6. Ding LH, Stilwell J, Zhang TT, Elboudwarej O, Jiang HJ, Selegue JP, et al. Molecular characterization of the cytotoxic mechanism of multiwall carbon nanotubes and nano-onions on human skin fibroblast. Nano Lett 2005;5(12):2448–2464. [PubMed: 16351195]
7. Lam CW, James JT, McCluskey R, Arepalli S, Hunter RL. A review of carbon nanotube toxicity and assessment of potential occupational and environmental health risks. Crit Rev Toxicol 2006;36(3): 189–217. [PubMed: 16686422]

8. Magrez A, Kasas S, Salicio V, Pasquier N, Seo JW, Celio M, et al. Cellular toxicity of carbon-based nanomaterials. Nano Lett 2006;6(6):1121–1125. [PubMed: 16771565]
9. Manna SK, Sarkar S, Barr J, Wise K, Barrera EV, Jejelowo O, et al. Single-walled carbon nanotube induces oxidative stress and activates nuclear transcription factor-kappa B in human keratinocytes. Nano Lett Sep;2005 5(9):1676–1684. [PubMed: 16159204]
10. Mu Q, Du G, Chen T, Zhang B, Yan B. Suppression of Human Bone Morphogenetic Protein Signaling by Carboxylated Single-Walled Carbon Nanotubes. ACS Nano 2009;3(5):1139–1144. [PubMed: 19402638]
11. Mu QX, Broughton DL, Yan B. Endosomal Leakage and Nuclear Translocation of Multiwalled Carbon Nanotubes: Developing a Model for Cell Uptake. Nano Lett Dec;2009 9(12):4370–4375. [PubMed: 19902917]
12. Qu GB, Bai YH, Zhang Y, Jia Q, Zhang WD, Yan B. The effect of multiwalled carbon nanotube agglomeration on their accumulation in and damage to organs in mice. Carbon Jul;2009 47(8):2060–2069.
13. Sayes CM, Gobin AM, Ausman KD, Mendez J, West JL, Colvin VL. Nano-C-60 cytotoxicity is due to lipid peroxidation. Biomaterials Dec;2005 26(36):7587–7595. [PubMed: 16005959]
14. Usenko CY, Harper SL, Tanguay RL. In vivo evaluation of carbon fullerene toxicity using embryonic zebrafish. Carbon Aug;2007 45(9):1891–1898. [PubMed: 18670586]
15. Sayes CM, Liang F, Hudson JL, Mendez J, Guo WH, Beach JM, et al. Functionalization density dependence of single-walled carbon nanotubes cytotoxicity in vitro. Toxicol Lett Feb;2006 161(2): 135–142. [PubMed: 16229976]
16. Mu QX, Liu W, Xing YH, Zhou HY, Li ZW, Zhang Y, et al. Protein binding by functionalized multiwalled carbon nanotubes is governed by the surface chemistry of both parties and the nanotube diameter. J Phys Chem C 2008;112(9):3300–3307.
17. Zhang B, Xing YH, Li ZW, Zhou HY, Mu QX, Yan B. Functionalized Carbon Nanotubes Specifically Bind to alpha-Chymotrypsin's Catalytic Site and Regulate Its Enzymatic Function. Nano Lett Jun; 2009 9(6):2280–2284. [PubMed: 19408924]
18. Zhou HY, Mu QX, Gao NN, Liu AF, Xing YH, Gao SL, et al. A nano-combinatorial library strategy for the discovery of nanotubes with reduced protein-binding, cytotoxicity, and immune response. Nano Lett 2008;8(3):859–865. [PubMed: 18288815]
19. Mu QX, Li ZW, Li X, Mishra SR, Zhang B, Si ZK, et al. Characterization of protein clusters of diverse magnetic nanoparticles and their dynamic interactions with human cells. Journal of Physical Chemistry C 2009;113(14):5390–5395.
20. Guldi DM, Prato M. Excited-state properties of C60 fullerene derivatives. Acc Chem Res 2000;33 (10):695–703. [PubMed: 11041834]
21. Berciaud S, Cognet L, Poulin P, Weisman RB, Lounis B. Absorption spectroscopy of individual single-walled carbon nanotubes. Nano Lett 2007;7(5):1203–1207. [PubMed: 17385932]
22. Worle-Knirsch JM, Pulskamp K, Krug HF. Oops they did it again! Carbon nanotubes hoax scientists in viability assays. Nano Lett 2006;6(6):1261–1268. [PubMed: 16771591]
23. Abassi YA, Jackson JA, Zhu J, O'Connell J, Wang XB, Xu X. Label-free, real-time monitoring of IgE-mediated mast cell activation on microelectronic cell sensor arrays. J Immunol Methods 2004;292(1–2):195–205. [PubMed: 15350524]
24. Solly K, Wang XB, Xu X, Strulovici B, Zheng W. Application of real-time cell electronic sensing (RT-CES) technology to cell-based assays. Assay Drug Dev Technol 2004;2(4):363–372. [PubMed: 15357917]
25. Decuzzi P, Ferrari M. The role of specific and non-specific interactions in receptor-mediated endocytosis of nanoparticles. Biomaterials 2007;28(18):2915–2922. [PubMed: 17363051]
26. Ahamed M, Karns M, Goodson M, Rowe J, Hussain SM, Schlager JJ, et al. DNA damage response to different surface chemistry of silver nanoparticles in mammalian cells. Toxicology and Applied Pharmacology 2008;233(3):404–410. [PubMed: 18930072]
27. Schins RPF, Duffin R, Hohr D, Knaapen AM, Shi T, Weishaupt C, et al. Surface modification of quartz inhibits toxicity, particle uptake, and oxidative DNA damage in human lung epithelial cells. Chemical Research in Toxicology 2002;15(9):1166–1173. [PubMed: 12230410]

28. Wang F, Gao F, Lan MB, Yuan HH, Huang YP, Liu JW. Oxidative stress contributes to silica nanoparticle-induced cytotoxicity in human embryonic kidney cells. Toxicol Vitro 2009;23(5):808–815.

29. Albright CD, Salganik RI, Craciunescu CN, Mar MH, Zeisel SH. Mitochondrial and microsomal derived reactive oxygen species mediate apoptosis induced by transforming growth factor-beta 1 in immortalized rat hepatocytes. J Cell Biochem 2003;89(2):254–261. [PubMed: 12704789]

30. Yang, H.; Wu, QY.; Tang, M.; Kong, L.; Xia, T.; Yin, HR., et al. Cytotoxicity and DNA-damage in mouse macrophage exposed to silica nanoparticles. In: Ding, JY.; Wang, XY.; Hong, Q.; Guo, WW.; Xin, XP., editors. 8th National Postgraduate Symposium on Environmental and Occupational Medicine, Proceedings; Shanghai: Shanghai Ctr Dis Control & Prevention; 2009. p. 100-105.

31. Huang DM, Hsiao JK, Chen YC, Chien LY, Yao M, Chen YK, et al. The promotion of human mesenchymal stem cell proliferation by superparamagnetic iron oxide nanoparticles. Biomaterials 2009;30(22):3645–3651. [PubMed: 19359036]

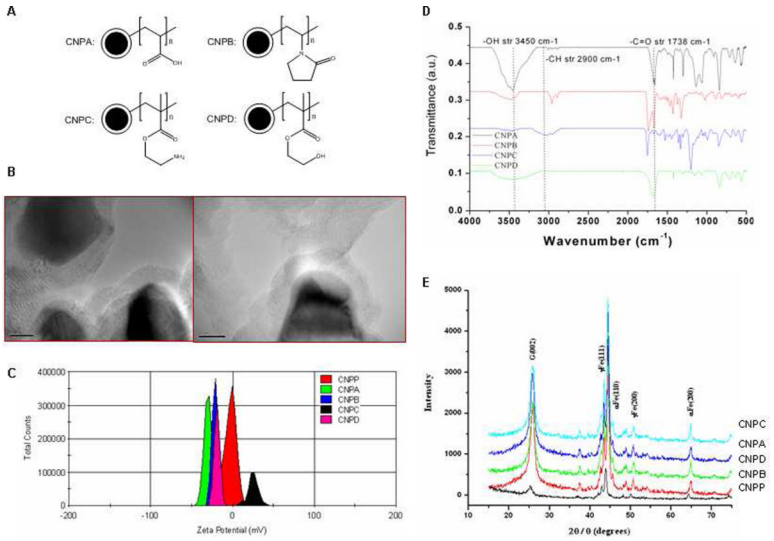

Figure 1.

Surface chemical structure and characterizations of various Fe@CNPs. A. Monomer structures of polymers coated on Fe@CNPs' surface; B. TEM micrographs of CNPC (left) and CNPD (right), respectively; C. ζ-potential measurement of five Fe@CNPs; D. FT-IR adsorption spectra of modified Fe@CNPs; E. XRD spectra of five Fe@CNPs.

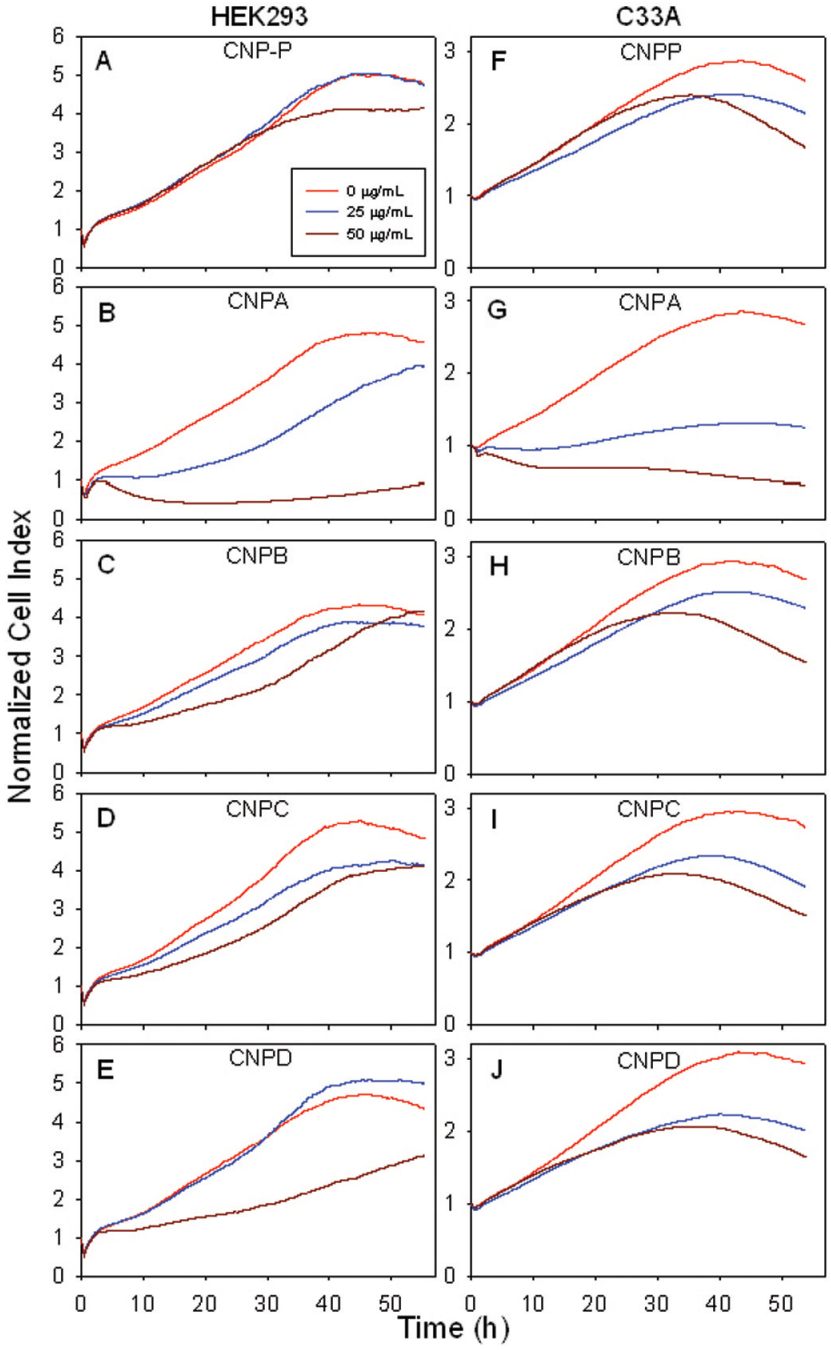

Figure 2.

Dynamic cellular responses of five Fe@CNPs. A–E, HEK293 cells; F–J, C33A cells. Cells were treated with Fe@CNPs for 25 (blue lines) and 50 (brown lines) μg/mL, respectively. Cell indices of the last time point before Fe@CNPs added were set to 1.0 and that time was set to zero. Cell growth curves were averaged from three individual measurements. Red lines indicate growth patterns of normal cells.

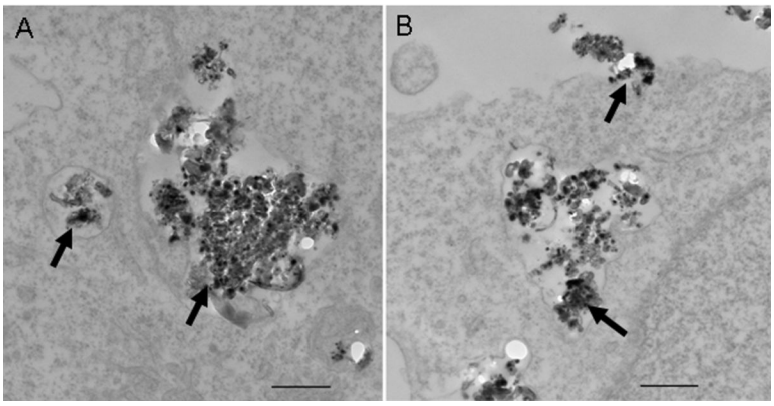

Figure 3.

TEM characterization of Fe@CNPs' uptake into C33A cells. A, CNPP; B, CNPA. Cells were treated with 400 μg/mL CNPP or CNPA at 37°C for 1 h, respectively. The cells were then fixed, embedded and sectioned followed by imaging. Arrows indicate Fe@CNPs and scale bars represent 100 nm.

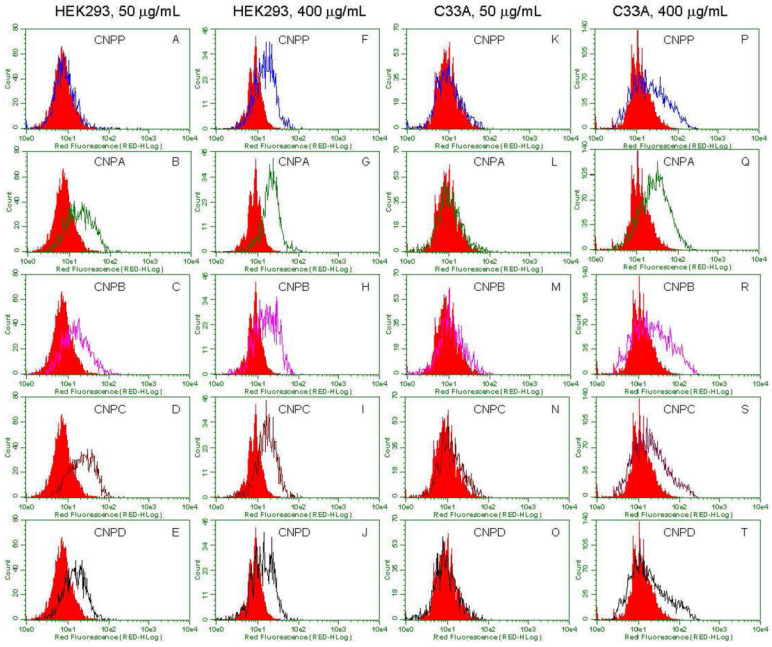

Figure 4.

ROS generation monitored by flow cytometry. HEK293 cells (A–J) and C33A cells (K–T) were treated with 50 and 400 μg/mL Fe@CNPs for 24 h, respectively. In these histogram plots, red filled regions indicate normal cell controls, unfilled regions indicate five Fe@CNPs treated cells, of which blue indicates CNPP, green indicates CNPA, pink indicates CNPB, brown indicates CNPC and black indicates CNPD.

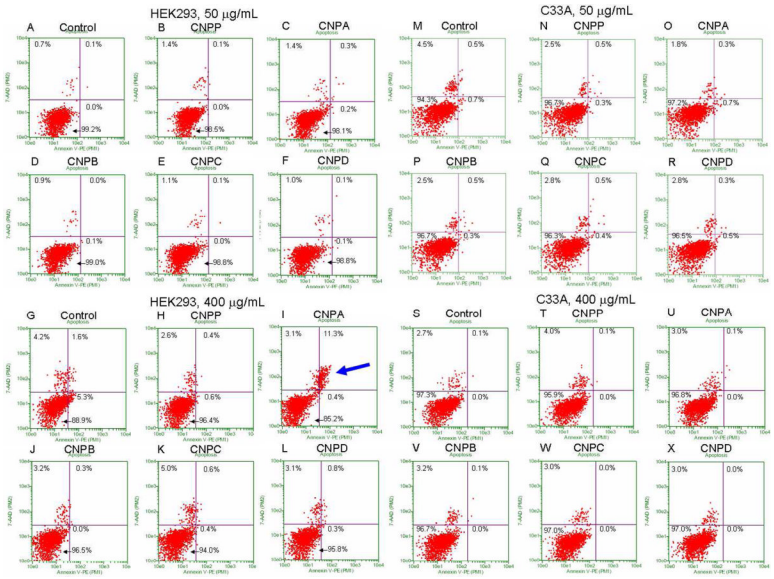

Figure 5.

Apoptosis detection by Annexin-V assay. HEK293 cells (A–L) and C33A cells (M–X) were treated with 50 and 400 μg/mL for 24 h, respectively. In four windows of each plot, the lower left indicates normal cells, the lower right indicates early apoptotic cells, the upper right indicates middle phase apoptotic cells and the upper left indicates late phase apoptotic cells or necrotic cells. Blue arrow indicates the apoptotic cells induced by CNPA at the concentration of 400 μg/mL.

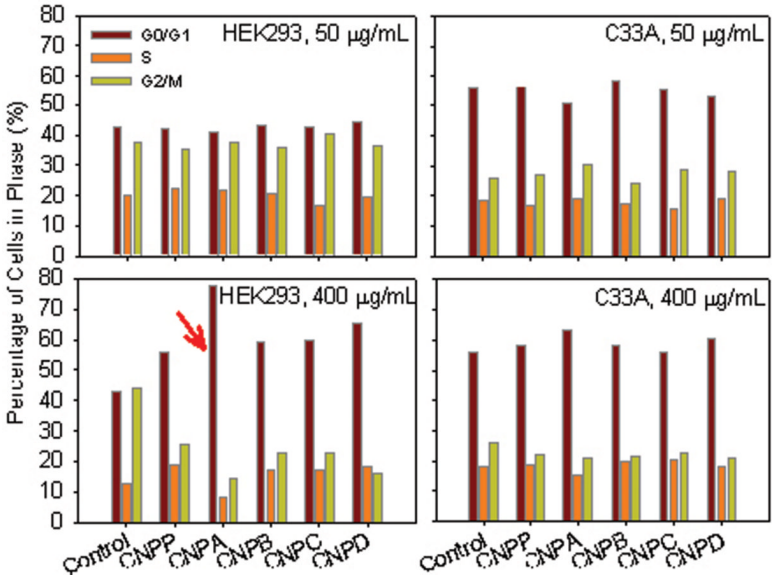

Figure 6.

Cell cycle analysis of HEK293 and C33A cells treated with 50 and 400 μg/mL Fe@CNPs for 24 h, respectively. Red arrow indicates the mostly affected cell sample as shown in Figure 5I.